Electrically switchable surface waves and bouncing droplets excited on a liquid metal bath

Xi Zhao,[1] Jianbo Tang,[2] and Jing Liu[1,2,*]

[1]*Key Laboratory of Cryogenics, Technical Institute of Physics and Chemistry, Chinese Academy of Sciences, Beijing 100190, China*
and School of Future Technology, University of Chinese Academy of Sciences, Beijing 100049, China
[2]*Department of Biomedical Engineering, School of Medicine, Tsinghua University, Beijing 100084, China*

(Received 9 September 2018; published 27 December 2018)

Metallic fluids may contain rather rich unconventional surface wave behaviors when subjected to specific forcing conditions. Here we introduce a high-surface-tension liquid metal–solution bilayer to the Faraday system and investigate its wave evolution under cylindrical confinement. Beyond the Faraday threshold, we observe the formation of highly symmetric wave patterns when the acceleration remains below an upper threshold value Γ_D, exceeding which gives rise to disordered wave patterns. By varying the driving frequency from 20 to 80 Hz, diverse wave patterns with fold symmetry from 2 to 10 are excited. We further show that noncoalescent droplets of the same liquid metal can be sustained on the structured wave patterns. Distant droplets can be confined at the antinodes of the wavy surface and self-assemble the corresponding wave structures. Besides outlining some major differences between the current system and conventional ones, we also demonstrate a simple yet fast method to switch the surface waves between different states by electrically altering the liquid metal surface tension.

DOI: 10.1103/PhysRevFluids.3.124804

I. INTRODUCTION

Faraday instability occurs when a fluid bath with a free upper surface is subjected to sufficient vertical vibration. When the vibration acceleration exceeds a critical value (the Faraday threshold), a flat hydrostatic surface becomes instantaneously unstable and parametric resonance of the surface wave appears [1]. The mechanism behind the emergence and pattern formation of Faraday waves is surprisingly sophisticated. Continuous efforts have been devoted to this classic system with considerable achievement made [2–7]. Still, satisfactory understanding regarding many aspects of the phenomenon is yet to be reached [4,5,8]. Although Faraday waves usually take highly irregular forms, stable yet symmetric wave patterns can be formed when critical conditions, certain driving frequency and acceleration, can be satisfied [2,9–15]. The study of Faraday waves has implications on the complex nonlinear dynamics and pattern formation theories of other hydrodynamic systems, such as Rayleigh-Bénard convection [16], and Taylor-Couette flow [17], as well as optical systems [18].

Faraday waves can be adjusted through controlling different variables of the system, for instance, driving conditions (e.g., driving frequency and amplitude), boundary conditions (e.g., container shape and meniscus), and fluid (e.g., fluid type and filling depth) [4,19]. Among them, the properties (viscosity, density, surface tension, etc.) of the filling fluid show significant influence on Faraday waves, in particular for the pattern formation [10,20,21]. In water systems, twofold

*jliu@mail.ipc.ac.cn

and fourfold symmetric patterns are observed [1]. While using oils with higher viscosity and lower surface tension, more complex patterns with pentagonal [9,11], hexagonal [11], octagonal [12], and dodecagonal [13] symmetry can be obtained. The surface tension of a fluid decides the boundary curvature of the contact region, and the surface waves emitted by this boundary meniscus will couple to the surface wave patterns, leading to further complicity [2,4,20]. In previous studies, such problem was usually avoided by brimful filling so that the contact line can be pinned at the container boundaries [13,22,23].

A vibrating fluid bath can be used as a platform to sustain and manipulate noncoalescent bouncing droplets of the same fluid. A Newton bearing force provided by a squeezed interlayer can prevent the coalescence between the droplet and the bath [24–26]. Consequently, a bouncing droplet can be kept for a long time and multiple bouncing droplets can self-assemble to form latticelike structures [8]. Moreover, the waves produced by the droplet impact can couple to the droplet motion and guide the droplet to "walk" horizontally [8,25,27–30]. Such hydrodynamic particle-wave association is found to give rise to intriguing dynamic droplet motions and surprising quantumlike behaviors [28,29]. Therefore, the motion of droplets deposited on a vibrating fluid bath has attracted widespread attention. Investigations with different fluids reveal different droplet behaviors due to the change in fluid properties [31–33].

In this study, we present experimental results of the Faraday waves and droplet behaviors carried out in a bilayer system composed of room-temperature liquid metal (liquid gallium-indium alloy) and NaOH solution. Compared to conventionally used water and oils, the present system represents a case with extreme fluid density and surface tension [34]. We investigate the acceleration region in which stable, periodic, and symmetrical Faraday wave patterns can be maintained in a frequency range from 20 to 80 Hz. We find that different frequencies may result in wave patterns of the same symmetry number but with different wave structures. In a global picture, however, the symmetry number correlates with the driving frequency. For the bouncing droplet experiments, we study both individual and collective droplet behaviors. We plot the bouncing regime diagram for individual droplet and find a narrow period-doubling region independent of droplet size. Multiple droplets deposited on the wave patterns above the Faraday threshold will bounce at the antinodes of the wavy surface so that the droplets collectively self-assemble to the symmetric wave structure. We demonstrate an exclusive electrocapillary method to swiftly switch the system between different states since the surface tension of the liquid metal can be altered by an applied electric field.

II. METHODS AND MATERIALS

Figure 1(a) shows the schematic setups of the experimental apparatus. The experimental system consists of a signal generator, a power amplifier, an electromagnetic shaker, and a piezoelectric accelerometer. The electromagnetic shaker (Yangzhou KeDong Co., Ltd., KDJ-100) has a maximum vibration amplitude of 15 mm and maximum vibration force of 1000 N. The signal generator (Tektronix, AFG 3051C) with a total harmonic distortion of 0.15% and phase noise of -110 dBc/Hz generates a sinusoidal signal which is amplified by the power amplifier (Yangzhou KeDong Co., Ltd., KD-5715) to drive the shaker. A circular glass container of 76 mm inner diameter for holding working fluid is firmly glued to the vibrating rod of the shaker. The motion of the container is ascribed as $a(t) = a\sin(2\pi ft)$, where a is the maximum of the acceleration, f the driving frequency, and $a(t)$ the acceleration measured by the piezoelectric accelerometer (Yangzhou KeDong Co., Ltd., 1020LC) fixed at the other end of the vibrator rod opposing the fluid bath. The accelerometer has a voltage sensitivity of 200 mV/g and typical error of 1% under the experimental conditions.

The liquid metal and the solution used in this study are eGaIn (eutectic gallium indium, 75.5% gallium and 24.5% indium by weight percent) and 0.25 mol/l NaOH solution, respectively. The filling depth of eGaIn and NaOH solution is 10 and 12 mm, respectively. The NaOH solution, which has a density of $\rho_E = 1009.5$ kg/m^3 and viscosity of $\nu_E = 1.1 \times 10^{-3}$ m^2/s, is used to eliminate an easily formed oxide film on the liquid metal surface, which hinders its fluidity [35]. In such

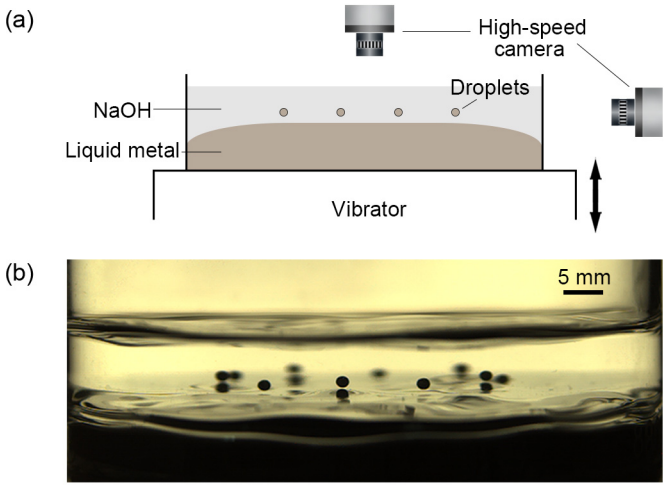

FIG. 1. (a) Schematic experimental setups; (b) droplets bouncing on the wavy liquid metal surface when the acceleration is beyond the Faraday threshold (see Video 1 of the Supplemental Material [36]).

alkaline environment, eGaIn has a density $\rho_{\mathrm{LM}} = 6280\ \mathrm{kg/m^3}$, kinematic viscosity $\nu_{\mathrm{LM}} = 3.2 \times 10^{-7}\ \mathrm{m^2/s}$, and interfacial tension $\sigma = 0.482\ \mathrm{N/m}$. Whenever needed, liquid metal droplets can be generated and merged to desirable size using a pipette and further removed through coalescing with the liquid metal bath. We set the frequency range of interest to 20–80 Hz.

The surface wave patterns are captured by an overhead high-speed camera (IDT, NR4.S3) with the assistance of a diffusion light source which is also illuminated from above the surface at a height of about 1 m. The camera is placed slightly inclined so that it will not capture its reflection on the liquid metal surface to facilitate observation clearness. To capture the vertical motion of bouncing droplets, the light source, container, and camera are aligned horizontally to take side view images. The distance of the droplet from the camera is adjusted to keep the droplet in focus, giving a total error in droplet diameter measurement of less than 0.014 mm. In order to ensure that the vibration strictly lies along the vertical axis and off-axis vibration is sufficiently minimized, the container is first carefully set horizontally on the vibrator platform using a level. Then we gradually increase the driving amplitude until a concentric-ring shaped surface wave pattern forms and we fine-tune the system so that the waves along a circle are of identical amplitudes (judged by eyesight). A representative side view of the system is shown in Fig. 1(b). It can be seen that bouncing droplets with well-defined distance can be sustained by the liquid metal bath when the Faraday threshold is surpassed and the surface is wavy.

III. RESULTS AND DISCUSSION

A. Threshold values of surface wave patterns

We first focus on the excitation of the surface waves. When the bath is subjected to vertical vibration, the gravity and the surface tension of the fluid act together as the restoring force in response to the reduced acceleration $\Gamma = a/g$, which measures the relative significance of the driving acceleration a to the gravitational acceleration g. Meanwhile, part of the input energy will be consumed due to dissipations at the fluid interface, interior, and boundaries [6,20]. At a given driving frequency f, the forced surface waves in our system are found to closely correlate to Γ and the surface vibration can be divided into three distinct states.

Gradually increasing Γ from the quiescent state, we observe the first threshold below which only concentric rings [Fig. 2(a)] are formed and the surface waves are harmonic. The

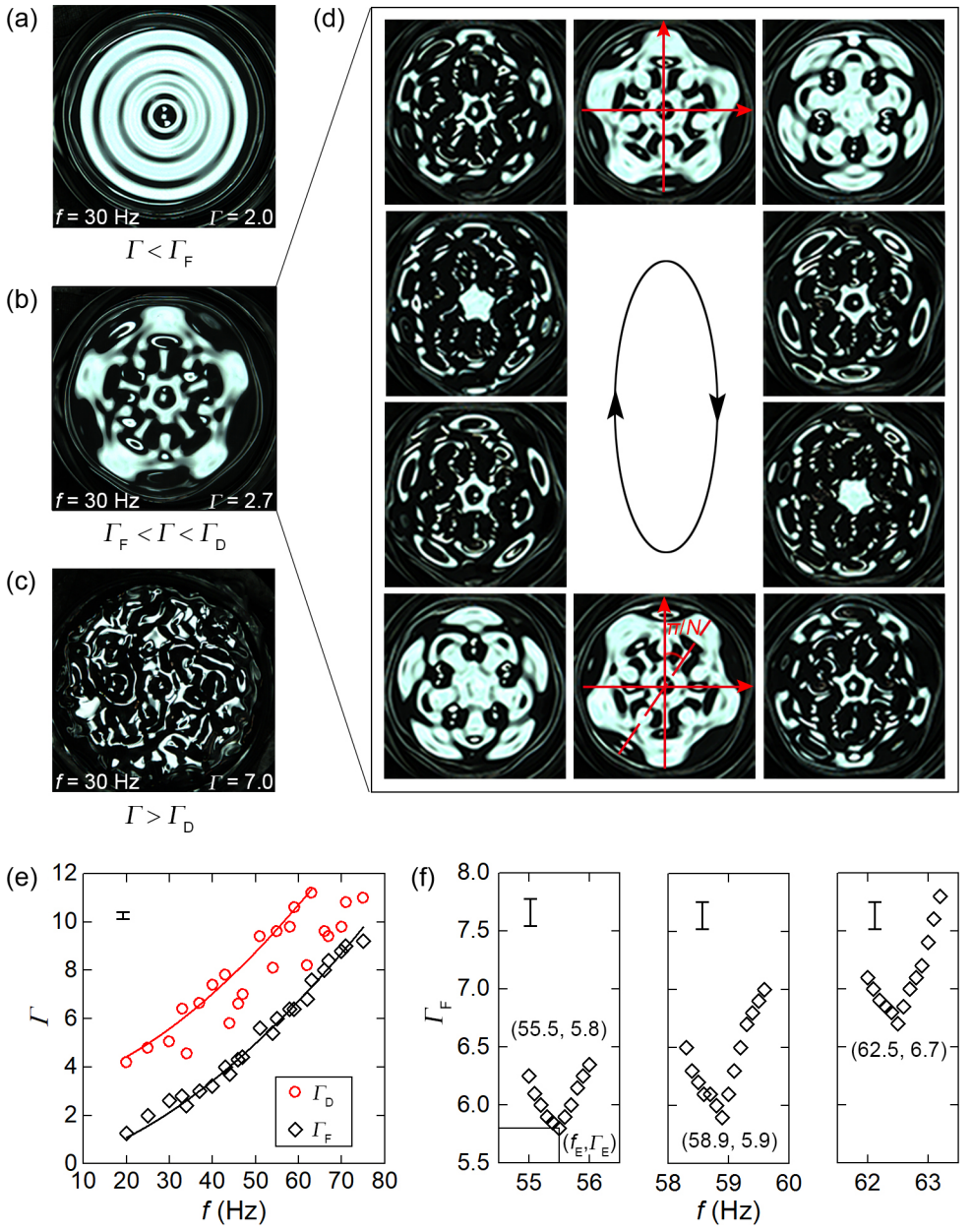

FIG. 2. Surface wave patterns formed when (a) $\Gamma < \Gamma_F$; (b) $\Gamma_F < \Gamma < \Gamma_D$; (c) $\Gamma > \Gamma_D$; (d) snapshots showing the evolution of a pentagonal wave pattern during one wave period ($f = 30$ Hz, $\Gamma = 2.7$; see Video 2 in the Supplemental Material [36]); (e) stability curves of Γ_F-f and Γ_D-f. The scatters represent the measured values while the solid lines in black and red are fitting curves of Γ_F and Γ_D, respectively. Note that both curves are fitted by a 5/3 power law and we exclude the wave competition cases during Γ_D fitting; (f) representative tongue-shape stability curves of Γ_F-f near the eigenfrequency f_E. Typical measurement uncertainties of acceleration are shown as error bars.

formation of the concentric rings in the liquid metal bath rather than a flat surface as observed in water and oil systems below the Faraday threshold is because the radius of the container (38 mm) is much smaller than the decay length of liquid metal in the whole frequency range

[$l_d = \sigma/(8\pi f \nu_{\mathrm{LM}}\rho_{\mathrm{LM}}) = 119$–$477$ mm], and the wave patterns will be significantly affected by the container sidewall and the meniscus structure [14,15].

Once the first threshold is reached, the ring patterns are overwhelmed by symmetric wave patterns of increasing wave amplitude [Figs. 2(b) and 2(d)]. The wave patterns consist of bright regions and dark regions. The bright regions seen in the wave patterns correspond to flat or almost flat liquid metal surface areas which can reflect most of the illuminating light back to the camera mounted over the bath, while the dark regions correspond to areas with significant slope which direct the illuminating light away from the camera. In the vibrating state with symmetric wave patterns, the wave motion becomes subharmonic (the wave frequency reduces to half the driving frequency) and therefore, this lower threshold corresponds to the Faraday threshold Γ_{F}. The existence of Γ_{F} can be understood as the critical energy input that needed to compensate system dissipations [20,21]. This means below Γ_{F}, the system dissipations consume all the input energy while beyond Γ_{F} excessive energy will be restored by gravitational force and surface tension, resulting in wave formation.

We note that the wave patterns beyond the Faraday threshold do not become instantaneously disordered. Instead, the vibrating surface develops highly symmetric wave patterns as the acceleration further increases. Figure 2(d) shows the time-lapse images of a pentagonal wave pattern driven by $f = 30$ Hz, $\Gamma = 2.7$ vibration. It appears that the wave pattern reveals its periodic structure after one driving period $1/f$, but the pattern is rotated by an angle defined by π/N, where N denotes the fold symmetry number of the wave pattern. We further find that this presentative rotation is indeed a switch between the surface elevations (wave crests) and surface depressions (wave troughs) after $1/f$. After two driving periods $2/f$, the nonrotated original wave pattern is restored, so the wave patterns evolving with half of the driving frequency (doubled period $T = 2/f$) are classified as subharmonic Faraday waves [1,20].

Further increasing Γ we reach a second threshold above which the entire symmetric wave patterns break into severely distorted Faraday waves featuring again the reduced frequency $f/2$ [Fig. 2(c)]. This upper threshold is referred to as the disorder threshold Γ_{D} [9,20,37].

We plot the two thresholds Γ_{F} and Γ_{D} over the driving frequency range $f = 20$–80 Hz [Fig. 2(e)]. Note that to measure the acceleration thresholds for surface waves, we first increase the driving acceleration to near but below the Faraday threshold and then we increase the acceleration at a stepwise increment of $\Delta\Gamma = 0.1$. For each adjustment, we wait for at least 2 min to ensure the waveform of the system is stabilized under that current acceleration. We observe an increasing trend for both Γ_{F} and Γ_{D} as we increase f. The Γ_{F}-f plots obtained from our system can be predicted by a similar relation which has been applied to other systems [8,14,26]:

$$\Gamma_{\mathrm{F}} = C_0(\rho_{\mathrm{LM}}/\sigma)^{1/3}\nu_{\mathrm{LM}}(2\pi f)^{5/3}, \tag{1}$$

where $C_0 = 45$ is a coefficient added to match the experimental results with the theoretical prediction. This value of C_0 is much larger than the previous report [8], which is mainly attributed to the dissipation enhancement caused by the bilayer configuration of the current system [22]. The Γ_{D} stability curve is shifted upwards in the Γ-f diagram but can still be fitted using the 5/3 power law. For some frequencies, the Γ_{D} value can be significantly lower than the mainstream which means the wave patterns become chaotic shortly after Γ_{F}. Such a situation appears since there exists more than one wave pattern in the system. The competition between different patterns promotes instability and thus decreases Γ_{D} [38,39]. It can also be found that the two stability curves of Γ_{F} and Γ_{D} divide the Γ-f diagram into three regions. One observes only concentric rings patterns below Γ_{F}, and in the region above Γ_{F} while still below Γ_{D}, Faraday waves with symmetric patterns emerge. Moving above the Γ_{D} threshold gives rises to disordered Faraday wave patterns.

Now we consider the shape of the Γ_{F}-f stability curve within a narrow frequency range. In Fig. 2(f), the results reveal the tongue shape of three stability curves which are prescribed by the Mathieu equation [2,6]. This means although the wave patterns vary as the driving frequency changes, the same wave pattern can be maintained within a frequency bandwidth which is found to be typically within 2 Hz. The critical frequency centered in the frequency bandwidth is known as the eigenfrequency f_{E} which corresponds to the lowest driving acceleration Γ_{E} required to hold the

pattern. For the frequency between two adjacent tongues, disordered waves form once the Faraday instability occurs since severe pattern competition exists under those driving conditions.

B. Frequency-dependent pattern selection

In this section, we show structured Faraday wave patterns formed within the acceleration range $\Gamma_F < \Gamma < \Gamma_D$ as the driving frequency varies. Figure 3(a) shows a series of wave patterns, with fold symmetry number N ranging from 2 to 10, that are produced in our experiments. It can be found that the structure and the fold symmetry number of wave patterns have a high dependence on the driving frequency. Increasing the driving frequency can lead to wave patterns with higher-fold symmetry number as well as higher complexity of the patterns. This is because the wave number k will increase when the driving frequency f is increased according to the dispersion relation [40]

$$\omega_0^2 = \frac{(\rho_{LM} - \rho_E)gk + \sigma k^3}{\rho_{LM}\coth(kh_{LM}) + \rho_E\coth(kh_E)}, \tag{2}$$

where $\omega_0 = 2\pi f$ is the eigenfrequency, and h_{LM} and h_E are the filling depth of the liquid metal and NaOH solution, respectively. The increasing trend of the wave number k, or equivalently, the decreasing trend of the wavelength $\lambda = 2\pi/k$, can be found by looking at the radial direction of the wave patterns as f increases.

Figure 3(b) plots the fold symmetry number N against the surveyed frequency range. Since the frequency bandwidth for the same mode is within 2 Hz, we conduct our experiments with 1 Hz stepwise increment. Note that by saying frequency-dependent pattern selection we not only mean f influences the structure of the wave patterns, but also we mean structured wave patterns can only be excited under discrete frequency values. In other words, structured wave patterns cannot be excited under some frequencies in our system. It can be found in the N-f diagram that while N generally increases as the increase of f, different f can result in the same N.

In Fig. 3(c), we compare four groups of wave patterns with the same $N(N = 5–8)$ obtained with different f. Looking at each horizontal row of Fig. 3(c), one finds wave patterns with the same N at discrete f but different structures. Switching to vertical rows, one observes a step increase of N of the wave patterns. We point out that the increments in f between adjacent cases are surprisingly matched both along the horizontal direction and the vertical direction, given the 2 Hz bandwidth. This can also be noticed from the parallel lines drawn in Fig. 3(b) to show the repeat of N as f increases. Patterns with the same fold symmetry number but different structures are also observed in other systems. One well-known example would be the vastly diverse sixfold snow crystals [41].

C. Bouncing liquid metal droplets

After a proper understanding of the surface waves formed on the liquid metal bath, we now couple bouncing droplets to the system. It is known that droplets can keep bouncing on a vibrating bath of the same fluid due to a bearing force provided by an interlayer which in the current case is the liquid layer of NaOH solution [24,26]. The bouncing behaviors of the droplets depend largely on driving parameters such as driving frequency and driving acceleration. Here we fix the driving frequency to 55 Hz and focus on the influence of driving acceleration. Note that we also change the driving acceleration at a stepwise increment of $\Delta\Gamma = 0.1$ and take a measurement after waiting for 2 min to ensure the droplet bouncing mode is stabilized at the new state. As shown in Fig. 4(a), we use the regime diagram introduced in Refs. [8,25,42,43] to classify the bouncing behaviors of the liquid metal droplets when deposited on a liquid metal bath. It should be noted that a vibrating bath acts as a droplet filter and a droplet can be sustained only when its size is located in a certain range [24]. This filter effect is influenced by both the fluid types and the operation conditions. Due to this filter effect, we are only able to sustain droplets with diameter ranges from 0.3 to 0.5 mm in the current system for $f = 55$ Hz.

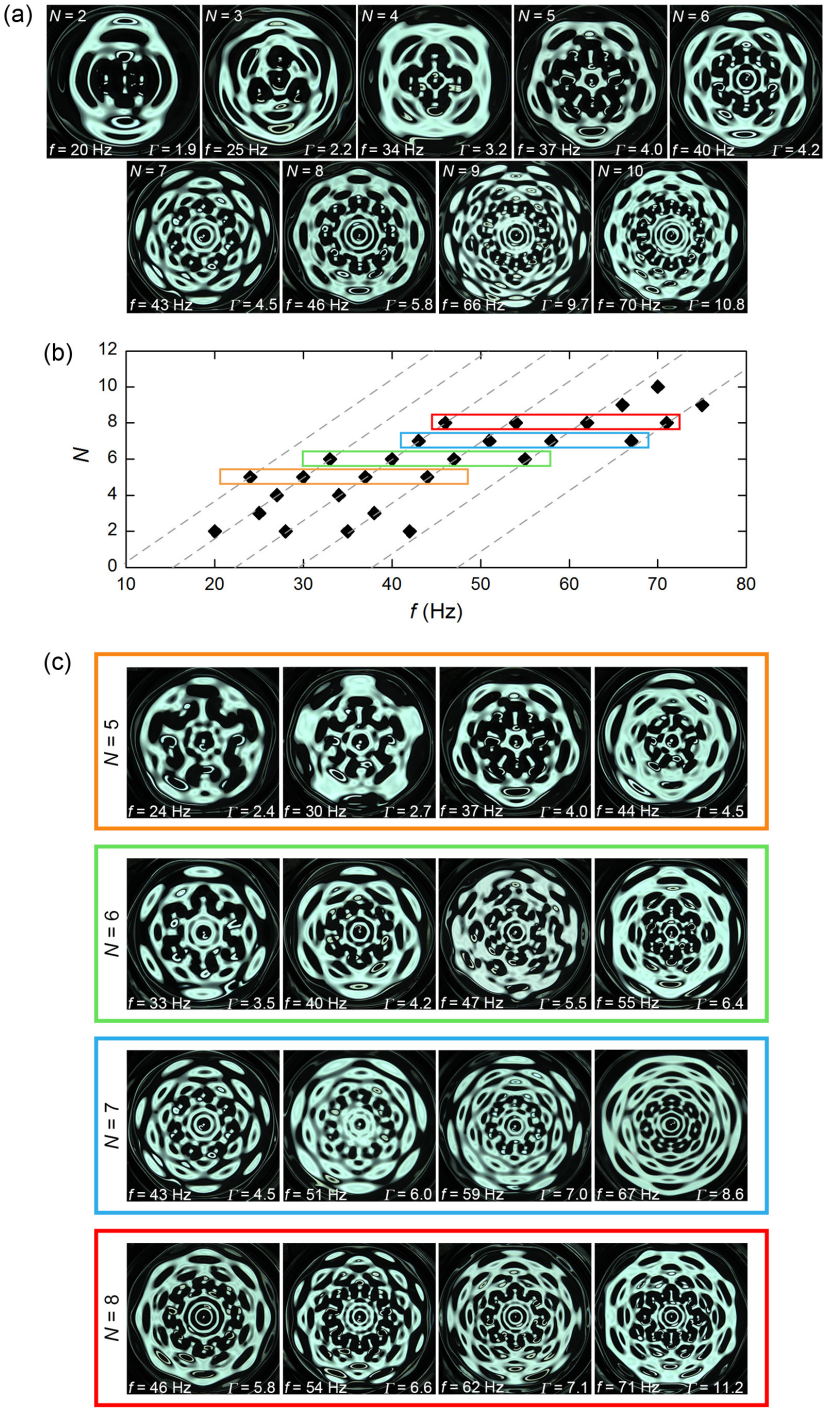

FIG. 3. (a) Faraday wave patterns with fold symmetry number N from 2 to 10 (see Video 3 in the Supplemental Material [36]); (b) plot of the fold symmetry number N against the driving frequency f. The parallel dashed lines are a guide for the eyes to show the repeat of N-f development; (c) four groups of Faraday wave patterns with the same N at different frequencies. Each group is identified by color in (b) (see Video 4 in the Supplemental Material [36]).

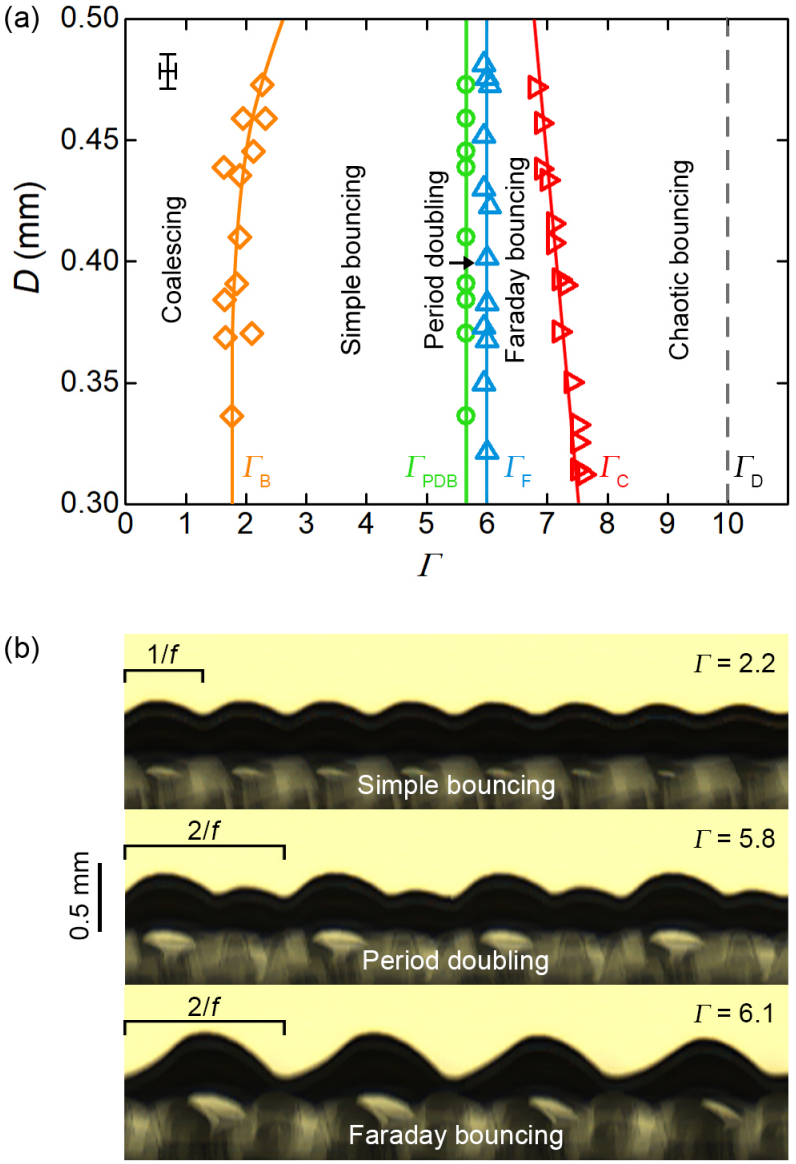

FIG. 4. (a) Regime diagram of liquid metal bouncing droplets; the driving frequency is fixed at 55 Hz. Typical measurement uncertainties of acceleration and droplet diameter are shown as error bars; (b) representative spatiotemporal diagrams showing the vertical trajectory of a liquid metal droplet in correspondence to the three stable bouncing states in (a): simple bouncing, period doubling, and Faraday bouncing (see Video 5 in the Supplemental Material [36]).

We identify five possible categories of bouncing behaviors and three of them result in stable bouncing [Figs. 4(a) and 4(b)]. The driving acceleration Γ should reach the lowest value, the simple bouncing threshold $\Gamma_B \sim 2$, required to sustain the droplets. Below Γ_B the droplets quickly coalesce with the bath. In this simple bouncing region, the droplets bounce in resonance with the bath vibration at a bouncing frequency equal to the driving frequency f; i.e., the droplet impacts the bath once during each wave period. Note that the effective acceleration felt by the droplet during impact will be altered since a circularly symmetric wave pattern exists. As Γ increases, droplet

bouncing becomes more energetic (higher bouncing height). When Γ reaches the period-doubling threshold Γ_{PDB}, the droplet changes its bouncing pace such that two successive bounces become alternately large and small and thus the bouncing period doubles. These two bouncing states (simple bouncing and period doubling) of the liquid metal droplets on the liquid metal bath recover the droplet bouncing behaviors found in other systems. However, in the current system, the regime diagram shows a wide simple bouncing region and a narrow period-doubling region, which differs largely from previous works. This means the simple bouncing state of the liquid metal droplets will not be altered in a wide acceleration range while the period-bouncing state can only be found in limited conditions close to but below the Faraday threshold Γ_{F}. In addition, for the fixed frequency here ($f = 55$ Hz), we never observe a complete period-doubling state (the "walking" state) and other intermittent states that are reported and extensively studied in previous works [8,25,42,43].

Inherent differences rise in the bouncing droplet experiments of the current system when $\Gamma > \Gamma_{\mathrm{F}}$. In water or oil systems, the emergence of disordered Faraday waves generally leads to immediate chaotic behavior followed by immediate coalescing of the droplets [8,25]. We find in our experiments that droplets can keep stable, long-term bouncing on the high-amplitude liquid metal Faraday waves when the Faraday instability occurs. The formation of symmetrical Faraday wave patterns in our system other than disordered waves should be preliminarily responsible for such Faraday bouncing state observed in our experiments. In this Faraday bouncing state, the droplets again impact the bath once per wave period, but since the frequency of the Faraday waves is half of the driving frequency, the droplet bouncing coupled to the Faraday waves also features the Faraday frequency $f_F = f/2$. The bouncing of the droplets in the Faraday bouncing region is greatly amplified. Further increasing the acceleration enters the chaotic bouncing region (defined by the chaotic bouncing threshold Γ_{C}) in which excited droplets will jump intermittently and chaotically across the bath. This indicates that chaotic behavior of the droplets occurs before the behavior of Faraday waves on the bath becomes disordered ($\Gamma_{\mathrm{D}} = 10$, $f = 55$ Hz). However, most droplets are found to stay long-term noncoalescent at the rim of the liquid metal bath.

Now one can find that the lower limit and upper limit of the system for stable droplet bouncing is Γ_{B} and Γ_{C}, respectively. For droplets of different size, the simple bouncing threshold Γ_{B} is found to be more significant for droplets with larger diameters, a circumstance also found in other systems [8,25], while no distinguishable size dependence of the period-doubling threshold Γ_{PDB} and the Faraday threshold Γ_{F} is measured under our current operation conditions. The chaotic bouncing threshold Γ_{C} shows a reverse proportional dependence to the droplet diameter, which implies larger droplets are more easily overexcited by the vibrating bath.

D. Self-assembly of bouncing droplets

As shown before, liquid metal droplets can be sustained when the Faraday waves are excited on the bath ($\Gamma_{\mathrm{F}} < \Gamma < \Gamma_{\mathrm{C}}$). In Fig. 5(a), we show that the bouncing droplets can be autonomously locked to the antinodes (maxima) of the Faraday wave patterns when deposited on the bath. As has been shown before, the droplet motion is forced to synchronize with the bath at half the driving frequency. A spatial argument for the lock effect is that droplets "impacting" on an inclined side of the wave patterns cannot be kept and will bounce off towards the wave trough. This is the mechanism for the horizontal motion of the walking droplets reported in other systems [27], but the waves, which are induced by droplet impact, are inherently different from the structured Faraday waves in our system. Eventually, the droplets will be confined at the sites of flat impact after repeated adjustment. Using high-speed imaging, we confirm that the impact of the droplets with the bath takes place when the antinodes become wave troughs. During one period of the synchronized motion, the droplets will be in flight when the antinodes become wave crests. As a result, neighboring droplets along the same circle bounce with opposite phases, i.e., a droplet's bouncing site corresponds to a wave crest while that of its neighbors corresponds to wave troughs.

Multiple droplets can be readily placed at the wave antinodes with one droplet bouncing at an antinode. Collectively, the droplets self-assemble stable symmetrical structures corresponding to the

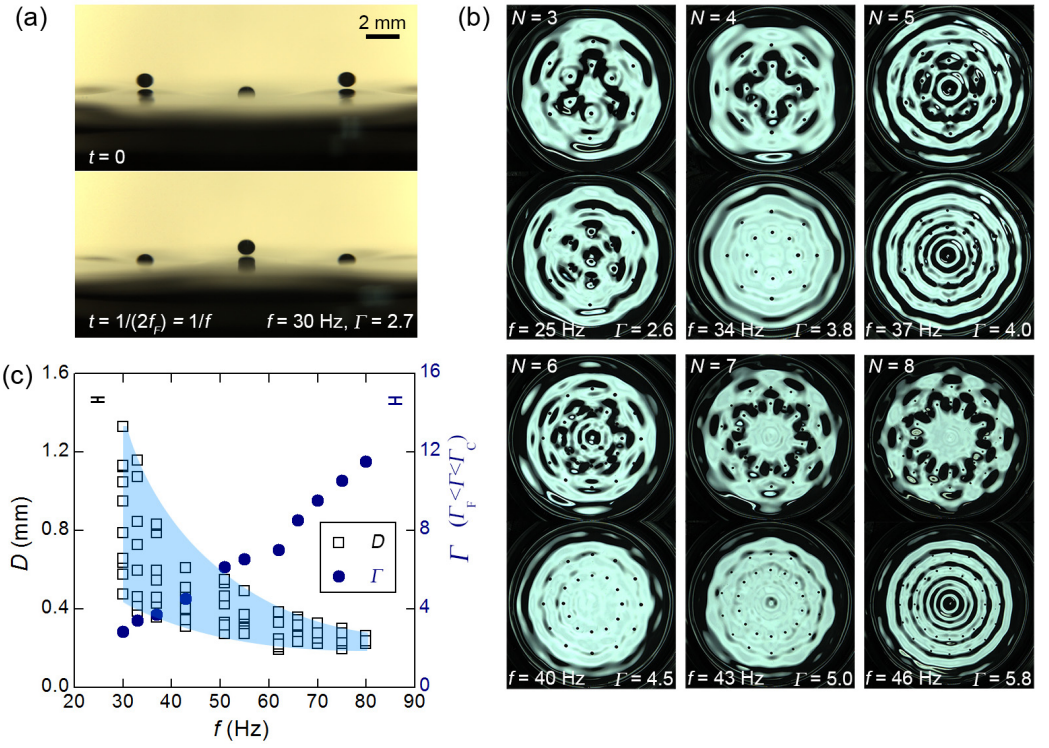

FIG. 5. Bouncing droplets on the vibrating liquid metal bath. (a) Droplets being locked at the wave antinodes and adjacent droplets bouncing in antiphase at the Faraday frequency f_F (equals half the driving frequency f) (see Video 6 in the Supplemental Material [36]); (b) Self-assemblies of liquid metal droplets at their Faraday bouncing state when the bath is vibrating with different fold symmetry number N (see Video 7 in the Supplemental Material [36]); (c) change of the diameter range of Faraday bouncing droplets that can be sustained as a function of f. The area filled in blue indicates the Faraday bouncing region. Γ is the driving acceleration corresponding to each surveyed driving frequency f, which is chosen from the acceleration range $\Gamma_F < \Gamma < \Gamma_C$ to maintain the stable Faraday bouncing state of liquid metal droplets. Typical measurement uncertainties of acceleration and droplet diameter are shown as error bars.

wave patterns on the bath. In Fig. 5(b) we show six cases with $N = 3$–8. For each case, two frames of different contrast during one wave period are selected to show the droplet self-assembly. Since both the crests and troughs can hold bouncing droplets, the number of the bouncing droplets along one ring equals the number of the antinodes of the wave patterns $2N$ (twice the fold symmetry number). Because different wave patterns can be constructed by varying the driving frequency (Fig. 3), different bouncing droplet assemblies can also be obtained accordingly. The antinodes in the middle of the radial direction on the circular bath [the two rings shown in Fig. 5(b)] are found to hold bouncing droplets easily while the inner region and the outer region of the bath are not so favorable for holding the droplets. The fact that the self-assembly of bouncing droplets formed in the current system stems from the structured Faraday wave patterns differs itself from the droplet arrays assembled by the waves induced by the droplets on the bath [8]. It can be found that the bouncing droplet self-assembly in the current system takes a long bonding distance (significantly larger than droplet-size scale). Such long-distance self-assembly represents one major difference from previous works where the bonding distance is short range (smaller or comparable to droplet-size scale).

The driving frequency f causes the difference in the droplet number $2N$ of the droplet assemblies; also it sets size restriction to the droplets which can be sustained by the bath due to the aforementioned filter effect. As shown in Fig. 5(c), we investigate the droplet diameter range on

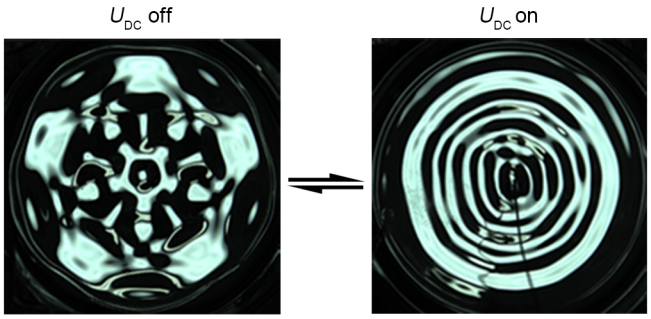

FIG. 6. Switchable manipulation of surface waves between different states with a dc voltage ($U_{dc} = 5$V, $f = 30$ Hz, $\Gamma = 2.7$). The cathode and the anode are inserted into the liquid metal layer and the NaOH solution layer, respectively (see Video 8 in the Supplemental Material [36]).

the Faraday wave patterns as a function of f. The result reveals a relatively wider diameter range with higher minimum and maximum for stable bouncing droplets under lower frequency. With the increase of f, both the minimum and the maximum decrease with the maximum dropping more quickly, accompanying with a gradual narrowing down of the diameter range. It can be inferred that droplets that are either too big or too small will be filtered by the bath and that the filter effect can be strengthened by increasing f. The conclusion can also be made that increasing f can lead to an increase in the assembled droplet number and a decrease in droplet size.

E. Electric manipulation

Since surface tension σ plays a determinative role in the formation of surface waves on a vibrating liquid bath, a feasible method to manipulate the surface waves is to alter the surface tension of the fluid. Distinct from traditional nonmetallic fluids, the unique nature of liquid metal is that its surface tension σ can be changed on demand through the electrocapillary effect rapidly and flexibly [44]. This exclusive feature of the liquid metal gives it the advantage to adjust the Faraday instability experiment and the bouncing droplet experiment electrically.

We demonstrate this concept by switching the surface waves of the liquid metal–alkaline bilayer system between different vibrating states. We simply insert the cathode (diameter $= 1$ mm) of a dc power source into the liquid metal bottom layer and the anode into the NaOH solution top layer. As shown in Fig. 6, a stable pentagonal Faraday wave pattern is excited under $f = 30$ Hz, $\Gamma = 2.7$ with the dc voltage U_{dc} cut off. Applying a low $U_{dc}(5\text{V})$ changes the wave patterns from structured Faraday wave patterns to concentric rings in 2–3 s. The change between bath vibrating states and its timescale require significant yet fast change in surface tension σ of the system.

The change in σ of the liquid metal–alkaline interface by the applied voltage follows the Lippman's principle [45]. A 5-V cathodic polarization has shown to be able to significantly reduce σ [44]. The reduction in σ increases Γ_F according to Eq. (1) so that the acceleration becomes insufficient to induce Faraday instability in the new state and the surface returns to concentric rings. The increase in fringe number of the rings confirms the reduction of σ when Eq. (2) is recalled. We further note that this electrical-manipulation method is switchable since its underlying electrocapillary mechanism is reversible. The wave can retain its initial pentagonal wave pattern when the dc voltage is cut off but with a longer time ($\sim$20 s).

IV. CONCLUSIONS

In summary, through introducing an unconventional metallic fluids system, we disclosed the formation of surface wave patterns and the behaviors of bouncing droplets by vertically vibrating

a cylindrical liquid metal bath. We clarify the differences of the current system with conventional Faraday instability experiments and bouncing droplet experiments:

(1) Highly symmetric Faraday wave patterns can be excited under well-defined acceleration ranges. Faraday wave patterns with fold symmetric number N ranging from 2 to 10 are obtained through frequency control. Surface wave patterns on the liquid metal surface are a superposition of meniscus waves (concentric circular waves) and parametrically forced Faraday waves since the decay length of liquid metal is much larger than the container radius.

(2) The regime diagram of liquid metal bouncing droplets acquired at $f = 55$ Hz shows a much narrower period-doubling region than a simple bouncing region ($1.8 < \Gamma_B < 5.7$ versus $5.7 < \Gamma_{PDB} < 6.0$). Liquid metal droplets are excited to enter a Faraday bouncing state right after a narrow period-doubling region. No transient states such as period-doubling cascade, intermittent horizontal movement, and walking behavior disclosed in traditional bouncing droplet studies are found in the liquid metal system under the conditions investigated.

(3) Liquid metal droplets can stably bounce on the vertically vibrating liquid metal bath surface at half the driving frequency above the Faraday threshold since structured surface wave patterns are formed. The Faraday bouncing state can be sustained in an acceleration range ($\Delta\Gamma \approx 1.0$) between the Faraday threshold and a chaotic bouncing threshold.

(4) The structured Faraday waves autonomously confine bouncing droplets at the antinodes and the droplets self-assemble to long-distance arrays in exact correspondence to the symmetric Faraday wave patterns.

(5) The wave patterns formed on the liquid metal bath can be readily switched between different states with a low dc voltage since its surface tension responds rapidly to external electrical polarization.

Our findings enrich the two classic experiments of Faraday instability and droplet bouncing, and are able to provide a general understanding of circumstances where liquid metal is evolved. The robust, frequency-dependent formation of complex structured Faraday waves and droplet assemblies with the liquid metal system makes it particularly suitable for studying pattern formation in fluid systems. In addition, being able to control the system with an applied electric field enables fast and on-demand manipulation via an extended degree of freedom, which is expected to bring alternative possibilities to the classic problems.

ACKNOWLEDGMENTS

This work is partially supported by the NSFC Key Project under Grant No. 91748206, Dean's Research Funding, and the Frontier Project of the Chinese Academy of Sciences.

X.Z. and J.T. contributed equally to this work.

[1] M. Faraday, On a peculiar class of acoustical figures; and on certain forms assumed by groups of particles upon vibrating elastic surfaces, Philos. Trans. R. Soc. London **121**, 299 (1831).

[2] S. Douady, Experimental study of the Faraday instability, J. Fluid Mech. **221**, 383 (1990).

[3] M. T. Westra, D. J. Binks, and V. D. W. Willem, Patterns of Faraday waves, J. Fluid Mech. **496**, 1 (2003).

[4] R. A. Ibrahim, Recent advances in physics of fluid parametric sloshing and related problem, J. Fluids Eng. **137**, 090801 (2015).

[5] J. Miles and D. Henderson, Parametrically forced surface waves, Annu. Rev. Fluid Mech. **22**, 143 (1990).

[6] T. B. Benjamin and F. Ursell, The stability of the plane free surface of a liquid in vertical periodic motion, Proc. R. Soc. A **225**, 505 (1954).

[7] F. Simonelli and J. P. Gollub, Surface wave mode interactions: Effects of symmetry and degeneracy, J. Fluid Mech. **199**, 471 (1989).

[8] S. Protière, A. Boudaoud, and Y. Couder, Particle wave association on a fluid interface, J. Fluid Mech. **554**, 85 (2006).
[9] M. Torres, G. Pastor, I. Jiménez, and F. Montero De Espinosa, Five-fold quasicrystal-like germinal pattern in the Faraday wave experiment, Chaos, Solitons Fractals **5**, 2089 (1995).
[10] R. A. Barrio, J. L. Aragón, C. Varea, M. Torres, I. Jiménez, and F. Montero de Espinosa, Robust symmetric patterns in the Faraday experiment, Phys. Rev. E **56**, 4222 (1997).
[11] J. Rajchenbach, D. Clamond, and A. Leroux, Observation of Star-Shaped Surface Gravity Waves, Phys. Rev. Lett. **110**, 094502 (2013).
[12] B. Christiansen, P. Alstrom, and M. T. Levinsen, Ordered Capillary-Wave States: Quasicrystals, Hexagons, and Radial Waves, Phys. Rev. Lett. **68**, 2157 (1992).
[13] W. S. Edwards and S. Fauve, Parametrically excited quasicrystalline surface waves, Phys. Rev. E **47**, R788 (1993).
[14] W. S. Edwards and S. Fauve, Patterns and quasi-patterns in the Faraday experiment, J. Fluid Mech. **278**, 123 (1994).
[15] B. A. Puthenveettil and E. J. Hopfinger, Evolution and breaking of parametrically forced capillary waves in a circular cylinder, J. Fluid Mech. **633**, 355 (2009).
[16] E. Bodenschatz, W. Pesch, and G. Ahlers, Recent developments in Rayleigh-Bénard convection, Annu. Rev. Fluid Mech. **32**, 709 (2000).
[17] G. I. Taylor, Stability of a viscous liquid contained between two rotating cylinders, Philos. Trans. R. Soc. London **223**, 289 (1923).
[18] H. M. Gibbs, S. L. McCall, and T. N. C. Venkatesan, Differential Gain and Bistability Using a Sodium-Filled Fabry-Perot Interferometer, Phys. Rev. Lett. **36**, 1135 (1976).
[19] M. C. Cross and P. C. Hohenberg, Pattern formation outside of equilibrium, Rev. Mod. Phys. **65**, 851 (2008).
[20] J. Bechhoefer, V. Ego, S. Manneville, and B. Johnson, An experimental study of the onset of parametrically pumped surface waves in viscous fluids, J. Fluid Mech. **288**, 325 (1995).
[21] D. M. Henderson, Effects of surfactants on Faraday-wave dynamics, J. Fluid Mech. **365**, 89 (1998).
[22] C. R. Tipton and T. Mullin, An experimental study of Faraday waves formed on the interface between two immiscible liquids, Phys. Fluids **16**, 2336 (2004).
[23] S. Douady and S. Fauve, Pattern selection in Faraday instability, EPL **6**, 221 (1988).
[24] Y. Couder, E. Fort, C. H. Gautier, and A. Boudaoud, From Bouncing to Floating: Noncoalescence of Drops on a Fluid Bath, Phys. Rev. Lett. **94**, 177801 (2005).
[25] J. Moláček and J. W. M. Bush, Drops bouncing on a vibrating bath, J. Fluid Mech. **727**, 582 (2013).
[26] D. Terwagne and J. W. M. Bush, Tibetan singing bowls, Nonlinearity **24**, R51 (2011).
[27] Y. Couder, S. Protière, E. Fort, and A. Boudaoud, Dynamical phenomena: Walking and orbiting droplets, Nature (London, UK) **437**, 208 (2005).
[28] Y. Couder, A. Boudaoud, S. Protière, and E. Fort, Walking droplets, a form of wave-particle duality at macroscopic scale, Europhys. News **41**, 14 (2010).
[29] J. W. M. Bush, Pilot-wave hydrodynamics, Annu. Rev. Fluid Mech. **47**, 269 (2015).
[30] M. Durey and P. A. Milewski, Faraday wave-droplet dynamics: Discrete-time analysis, J. Fluid Mech. **821**, 296 (2017).
[31] T. Gilet, N. Vandewalle, and S. Dorbolo, Controlling the partial coalescence of a droplet on a vertically vibrated bath, Phys. Rev. E **76**, 035302 (2007).
[32] T. Gilet, D. Terwagne, N. Vandewalle, and S. Dorbolo, Dynamics of a Bouncing Droplet onto a Vertically Vibrated Interface, Phys. Rev. Lett. **100**, 167802 (2008).
[33] G. Pucci, E. Fort, A. M. Ben, and Y. Couder, Mutual Adaptation of a Faraday Instability Pattern with its Flexible Boundaries in Floating Fluid Drops, Phys. Rev. Lett. **106**, 024503 (2011).
[34] X. Zhao, J. B. Tang, and J. Liu, Surfing liquid metal droplet on the same metal bath via electrolyte interface, Appl. Phys. Lett. **111**, 101603 (2017).
[35] Q. Xu, N. Oudalov, Q. Guo, H. M. Jaeger, and E. Brown, Effect of oxidation on the mechanical properties of liquid gallium and eutectic gallium-indium, Phys. Fluids **24**, 063101 (2012).

[36] See Supplemental Material at http://link.aps.org/supplemental/10.1103/PhysRevFluids.3.124804 for videos.
[37] N. B. Tufillaro, R. Ramshankar, and J. P. Gollub, Order-Disorder Transition in Capillary Ripples, Phys. Rev. Lett. **62**, 422 (1989).
[38] S. Ciliberto and J. P. Gollub, Pattern Competition Leads to Chaos, Phys. Rev. Lett. **52**, 922 (1984).
[39] S. Ciliberto and J. P. Gollub, Chaotic mode competition in parametrically forced surface waves, J. Fluid Mech. **158**, 381 (1985).
[40] K. Kumar and L. S. Tuckerman, Parametric instability of the interface between two fluids, J. Fluid Mech. **279**, 49 (1994).
[41] K. G. Libbrecht, The physics of snow crystals, Rep. Prog. Phys. **68**, 855 (2005).
[42] Ø. Wind-Willassen, J. Moláček, D. M. Harris, and J. W. M. Bush, Exotic states of bouncing and walking droplets, Phys. Fluids **25**, 082002 (2013).
[43] L. D. Tambasco, J. J. Pilgram, and J. W. M. Bush, Bouncing droplet dynamics above the Faraday threshold, Chaos **28**, 096107 (2018).
[44] J. B. Tang, X. Zhao, Y. Zhou, and J. Liu, Triggering and tracing electro-hydrodynamic liquid-metal surface convection with a particle raft, Adv. Mater. Interfaces **4**, 1700939 (2017).
[45] F. Mugele and J. C. Baret, Electrowetting: From basics to applications, J. Phys.: Condens. Matter **17**, R705 (2005).